Investigation of the generalization capability of a generative adversarial network for large eddy simulation of turbulent premixed reacting flows

Investigation of the generalization capability of a generative adversarial network for large eddy simulation of turbulent premixed reacting flows

L. Nista[a,*], C. D. K. Schumann[a], T. Grenga[a], A. Attili[b], H. Pitsch[a]

[a] *Institute for Combustion Technology, RWTH Aachen University, Aachen, 52056, Germany*
[b] *Institute for Multiscale Thermofluids, School of Engineering, University of Edinburgh, Edinburgh, EH9 3FD, United Kingdom*

Abstract

In the past decades, Deep Learning (DL) frameworks have demonstrated excellent performance in modeling non-linear interactions and are a promising technique to move beyond physics-based models. In this context, super-resolution techniques may present an accurate approach as subfilter-scale (SFS) closure model for Large Eddy Simulations (LES) in premixed combustion. However, DL models need to perform accurately in a variety of physical regimes and generalize well beyond their training conditions. In this work, a super-resolution Generative Adversarial Network (GAN) is proposed as closure model for the unresolved subfilter-stress and scalar-flux tensors of the filtered reactive Navier-Stokes equations solved in LES. The model trained on a premixed methane/air jet flame is evaluated a-priori on similar configurations at different Reynolds and Karlovitz numbers. The GAN generalizes well at both lower and higher Reynolds numbers and outperforms existing algebraic models when the ratio between the filter size and the Kolmogorov scale is preserved. Moreover, extrapolation at a higher Karlovitz number is investigated indicating that the ratio between the filter size and the thermal flame thickness may not need to be conserved in order to achieve high correlation in terms of SFS field. Generalization studies obtained on substantially different flame conditions indicate that successful predictive abilities are demonstrated if the generalization criterion is matched. Finally, the reconstruction of a scalar quantity, different from that used during the training, is evaluated, revealing that the model is able to reconstruct scalar fields with large gradients that have not been explicitly used in the training. The a-priori investigations carried out assess whether out-of-sample predictions are even feasible in the first place, providing insights into the quantities that need to be conserved for the model to perform well between different regimes, and represent a crucial step toward future embedding into LES numerical solvers.

Keywords: Large Eddy Simulation; Generative Adversarial Network; Premixed Combustion Modeling; Data-Driven Modeling; Generalization Capability

1. Introduction

Large Eddy Simulations (LES) are essential for the design of future energy-conversion systems due to their superior accuracy and still affordable computational cost in capturing high-order features (e.g., turbulence-combustion interaction, mixing behavior, etc.) compared to the most widely used Reynolds Averaged Navier-Stokes (RANS) approach [1]. In LES, the flow field is decomposed into the explicitly resolved flow and the unresolved subfilter-scale (SFS) flow. The filtering operation results in unclosed terms (e.g., subfilter-scale stress tensor term (momentum), subfilter scalar-flux and filtered chemical source terms (scalar-transport equation), etc.,) that must be modeled. In the past decades, considerable attention has been paid to LES closure model developments through algebraic-based equations [2]. Recently, Deep Learning (DL) techniques have performed well in modeling non-linear flow interactions, and thus hold the promise of advancing modeling and analyzing the intricate structures associated with turbulent reacting flows [3, 4]. The usage of DL methods for LES closure models has been identified as one of its key applications by the fluid dynamics community [5]. The new models are typically evaluated a-priori, which means that modeled SFS terms are compared with the exact solution computed from Direct Numerical Simulations (DNS).

A-priori studies have been performed to demonstrate that Neural Networks (NN) can be potentially suitable to close equations in the context of turbulence combustion [3]. Vollant *et al.* [6] considered an ANN to predict the subgrid-scalar mixing using the optimal estimation theory. Seltz *et al.* [7] trained a Convolutional Neural Network (CNN) model for the prediction of the filtered progress variable source term, Yellapantula *et al.* [8] employed a deep Artificial Neural Network (ANN) to predict the scalar dissipation rate, and similarly, Yao *et al.* [9] used an ANN for the closure of the conditional scalar dissipation rate in turbulent spray flames, all demonstrating good agreement with the DNS data. Lapeyre *et al.* [10] used a CNN architecture to estimate the subfilter-scale wrinkling in turbulent premixed flames. These a-priori investigations have shown that their configurations were able to achieve very high accuracy in predicting unresolved fields, usually outperforming conventional models at similar conditions to the ones used for training.

Less attention has been devoted to the modeling of the unresolved subfilter-scale stress tensor and the unresolved scalar flux, for which Super-Resolution (SR) techniques can be used to reconstruct high-resolution (e.g., DNS) from low-resolution flow fields (e.g., LES). The SR research field has received substantial attention from the computer vision research community and has a wide range of applications. Early works based on SRCNN have shown excellent performance in producing images with outstanding visual quality [11]. In this view, Ledig *et al.* [12] proposed a novel architecture, the Super-Resolution Generative Adversarial Network (SRGAN), using perceptual and adversarial losses to favor outputs residing on the manifold of natural images. Thanks to their distinguished capabilities, several of those architectures have been recently applied for closure modeling [4]. In the context of LES modeling, the work of Fukami *et al.* [13] demonstrated the ability to use deep CNNs to super-resolve three-dimensional incompressible turbulent flows solely from the coarse-grained data fields, enhancing subfilter physical structures. Hassanaly *et al.* [14] demonstrated how an adversarial approach can be used to sample conditional high-dimensional distributions for the deconvolution of turbulent atmospheric flow data. Recently, Bode *et al.* [15] presented a novel Physics-Informed Enhanced Super Resolution Generative Adversarial Network (PIESRGAN), which was trained with unsupervised DL using adversarial and physics-informed losses. With this approach, the authors were able to match the energy and scalar spectra of homogeneous isotropic turbulence DNS nearly perfectly and demonstrated the model's ability to work in an a-posteriori context.

However, ML-based approaches might perform poorly when applied to configurations substantially different from those they were trained on, as data from different regimes is usually absent from the training dataset and the prediction of the networks are entirely data-driven [16]. This might cause convergence issues in a-posteriori applications, as suggested by Lapeyre *et al.* [17]. Attili *et al.* [18] and Xing *et al.* [19], using similar architectures, performed some preliminary a-priori generalization studies. Their work demonstrated that the CNNs can be trained on canonical simple cases and applied to practical configurations indicating good extrapolation capabilities. Another potential drawback of data-based ML models is that highly-resolved data needed for the training is available only at a relatively low Re number compared to real applications (e.g., gas-turbine combustors) due to the prohibitive cost of DNS. Without generalization capabilities, the supervised data-driven models are limited to physical conditions for which DNS data or highly-resolved LES is available [4].

In this work, a SR Generative Adversarial Network (GAN) [20], is employed as closure model for the unresolved Reynolds-stress and scalar-flux tensors. The filtered momentum equation reads [2]

$$\frac{\partial \overline{\rho}\,\widetilde{u}_i}{\partial t} + \frac{\partial \overline{\rho}\,\widetilde{u}_i\widetilde{u}_j}{\partial x_i} = -\frac{\partial \overline{p}}{\partial x_j} + \frac{\partial \overline{\tau}_{ij}}{\partial x_i} - \frac{\partial\,\overline{\rho}\,\tau^r_{ij}}{\partial x_i}, \quad (1)$$

where the unresolved stress tensor τ^r_{ij} is given by

$$\tau^r_{ij} = (\widetilde{u_i u_j} - \widetilde{u}_i\,\widetilde{u}_j). \quad (2)$$

Similarly, in the filtered temperature transport equation, τ^T_i is the unresolved scalar flux defined as

$$\tau^T_i = (\widetilde{u_i T} - \widetilde{u}_i\,\widetilde{T}), \quad (3)$$

but the same argument can applied to any scalar quantity (in the rest, for the sake of brevity, the mass-weighted filtering $\tilde{\cdot}$ is indicated by the simple filtering operation $\bar{\cdot}$). The proposed method uses the generator of a GAN architecture to reconstruct the high-resolution field (DNS) from the lower-resolution F-DNS field (LES-like), so that Eq. (2) and Eq. (3) can be evaluated directly at the DNS level. The a-priori investigations reported in this work consider the Filtered-DNS (F-DNS) field to be statistically similar to an LES field.

As limitations with respect to generalizability are largely unexplored, the aim of the work is to investigate the ability to generalize to flow conditions that are different from the training data. First, analyses are devoted to the investigation of the model's capability to extrapolate towards higher and lower Re numbers. Moreover, a-priori extrapolation capabilities at a higher Karlovitz number on a similar and a different configuration are analyzed. In addition, the reconstruction of a scalar quantity, specifically not included during the training, is investigated to assess the generalization towards different physical quantities. Finally, the implication of the results obtained are discussed.

2. DNS Dataset

The training of the GAN architecture is only performed on the R2K1 configuration, which is part of a DNS dataset composed of four premixed methane/air turbulent slot jet flames, produced by Luca *et al.* [21]. This dataset includes DNSs at four different Reynolds numbers with approximately constant Kolmogorov scale η. A summary of all relevant flow parameters is provided in Table 1. Turbulent premixed planar jet flames with equivalence ratio $\phi = 0.7$ at unburnt temperature of $800K$ and pressure of 4 *atm*, bulk velocity U of $100\ m/s$ and surrounded by a coflow with composition equivalent to the fully burnt mixture are considered. The computational domain is sized $24H$ in the streamwise x, $16H$ in the cross-stream y, and $4.3H$ in the spanwise z direction. Periodic boundary conditions were applied in the spanwise directions, open boundary conditions were imposed at the outlet and, no-slip conditions were prescribed at the crosswise boundaries. The grid resolution is uniform in all directions, with $dx = dy = dz = 20\ \mu m$ for all four DNS. The laminar flame speed is $S_L = 1\ m/s$ while the thermal flame thickness is $\delta_L = 110\ \mu m$. This leads to $dx/\eta < 2$ and thus $\delta_L/dx \approx 6$. DNS data were extracted after a statistically stable state has been reached. The training is comprised exclusively of data from the R2K1 simulation, whereas the flames R1K1, and R4K1 are considered only as test datasets for a-priori evaluations.

To investigate the generalization at different Karlovitz number, an additional turbulent premixed jet flame of methane/air with similar flow conditions to the R2K1 configuration but higher Karloviz number is considered, i.e., R2K2 [23]. This turbulent premixed jet flame has an unburnt temperature of $500\ K$ and a pressure of $4\ bar$. The grid size is uniform such that $dx/\eta < 2$, equivalent to the previous series of DNS and the $\delta_L/dx \approx 15$. The laminar flame speed is $S_L = 0.25\ m/s$.

Furthermore, a similar turbulent premixed planar jet flame with a hydrogen/air mixture, called H2K2, at $Re = 5000$ and $Ka = 43.5$ [22, 24] is considered to assess generalization capabilities to different configurations and flame properties. It is composed of a central jet of a gaseous mixture of hydrogen and oxygen at stoichiometric equivalence ratio. For this mixture, the thermal flame thickness is $\delta_L = 435\ \mu m$, and the laminar flame speed $S_L = 1.195\ m/s$. Further characterization of the turbulence statistics can be found in [22].

3. Methodology and neural network architecture

3.1. Generative adversarial network architecture

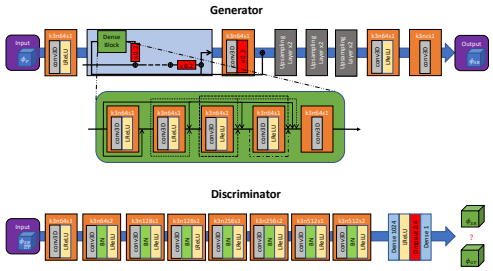

Fig. 1: The structure of the generator (above) and the discriminator (below) of the GAN architecture. ϕ_F indicates the filtered field, ϕ_{SR} is the super-resolved field, and ϕ_{GT} refers to the ground-truth field. Moreover, k is the kernel size, n is the number of filter maps, and s is the strides along each spatial dimension.

The GAN employed in this work, schematically shown in Fig. 1, is composed of two different CNNs, a generator, and a discriminator, already introduced in previous work [20] and designed for physical applications. Based on the PIESRGAN architecture developed by Bode *et al.* [15], both generator and discriminator heavily rely on the use of three-dimensional Convolutional Layers (CL) with leaky rectified linear units as activation functions, in contrast to the original ESRGAN structure [11] which relies on two-dimension CLs.

The generator aims to increase information content of the low-resolution input and learn all relevant complex transformations to map the input to the high-resolution output. This is efficiently achieved by the usage of residual-in-residual dense blocks (RRDB) and skip-connections [11]. In this architecture, there is only one RRDB compared to the 23 RRDBs employed in the original ESRGAN [11]. After the extraction of distinct level features, differently to the PIESRGAN structure, three upsampling layers are

Table 1: Simulation parameters of the premixed methane/air and hydrogen/air turbulent flames [21, 22], evaluated in the fully turbulent region. H is the inlet slot width, Ka is the Karlovitz number, and u' is the turbulent velocity fluctuation.

	R1K1	R2K1	R2K2	R3K1	R4K1	H2K2
Re [-]	2800	5600	5600	11200	22400	5000
U [*m/s*]	100	100	90	100	100	93
H [*mm*]	0.6	1.2	0.8	2.4	4.8	1.08
Ka [-]	39	23	240	21	21	43.5
u'/S_L [-]	14.2	10.0	35.0	9.8	11.6	7.85
η [μm]	18	23	13	25	25	10.2
δ_L [μm]	110	110	200	110	110	444

employed to consistently increase the input dimensions by a factor of 8 in each spatial direction. Each layer doubles the dimensions of the input by nearest neighbor interpolations to replicate consecutive grid points, followed by a convolutional layer to improve the approximation [11]. The number of filter maps for each CL is constant and set to 64. The total number of trainable parameters of the generator is around 25 million with 4 channels (variables).

The discriminator is a CNN with binary classification output, which provides non-linear feedback to the generator on the quality of the field produced. The discriminator network structure is kept unchanged compared to the PIESRGAN implementation, switching from two-dimensional to three-dimensional CLs compared to the original ESRGAN architecture. The number of filter maps doubles for each CL starting at 64.

The original perceptual loss introduced on the ESRGAN implementation [11] is replaced by a combination of three loss functions: the pixel loss ($\mathrm{L_{pixel}}$), the pixel gradient loss ($\mathrm{L_{gradient}}$), and the relativistic average discriminator loss ($\mathrm{L_{RaGAN}}$) (its precise definition can be found in [11]:

$$\begin{aligned} \mathrm{L_{gen}} &= \beta_1 \mathrm{L_{pixel}} + \beta_2 \mathrm{L_{gradient}} + \beta_3 \mathrm{L_{RaGAN}} \\ \mathrm{L_{pixel}} &= MSE(\phi_{SR}, \phi_{DNS}) \\ \mathrm{L_{gradient}} &= MSE(\vec{\boldsymbol{\nabla}}\phi_{SR}, \vec{\boldsymbol{\nabla}}\phi_{DNS}), \end{aligned} \tag{4}$$

where the coefficients $\beta = [0.89, 0.06, 0.00006]$ were previously tuned [20]. The Mean-Squared Error (MSE) is computed between the reconstructed (SR) and the ground-truth (DNS) fields, as indicated in Eq. 4. The MSE operator is applied separately to all elements when tensor quantities are considered. The L_1 norm is applied to each component of the loss function to drive the network's optimization. The generator, initialized with random weights, is pre-trained using only pixel loss and without the adversarial component to prevent GAN convergence failure [20]. Subsequently, the pre-trained generator is used to initialize the GAN training, and trained until no additional improvement on the reconstructed field is observed.

3.2. Training strategy

As all the DNS were performed on domains much larger than the flames themselves, only relevant subsections of each domain are considered for training and testing. In order to obtain flow fields comparable to those obtained from LES simulations, all the DNS flames are downsampled using a box filter with width $\Delta = 8\,dx$. The training is then performed only using the R2K1 dataset. Due to the impracticable, large computational domain compared to the available GPU memory, training and validation processes employed randomly extracted sub-boxes with size 64^3 and 8^3 for high- and low-resolution fields, respectively. A total of 73100 boxes are used for the training, where the last 10% of the available snapshots are not included in the training dataset as they are used for validation and testing purposes. To prevent overfitting, data augmentation is considered by randomly flipping and rotating the sub-boxes. Each dataset includes various physical quantities, such as the velocity components (U, V, W) and various scalar fields, such as the temperature T and OH mass fraction, although not all fields are considered for training. The model is trained using all velocity components and a single scalar field, the temperature, as indicated in Eq. 5. Both velocity components and scalar quantity of high- and low-resolution data are normalized with their global (i.e., computed using all snapshots) maximum and minimum to augment the network's performance. The generator performs then a consistent upsampling of the input variables proportional to the upsampling factor:

$$\begin{aligned} (U, V, W, T) =& \mathbf{f}_{generator}(\overline{U}, \overline{V}, \overline{W}, \overline{T}) \\ \mathbf{f}_{generator}: \;& \mathbb{R}^{\Omega} \rightarrow \mathbb{R}^{\Omega x 8^3}, \end{aligned} \tag{5}$$

where Ω is a regular three-dimensional F-DNS grid, $x8$ is the upsampling factor employed in each direction, and the input/output variables are normalized consistently. The input/output quantities are schematically reported in Fig. 1.

Given the large number of boxes available as well as the deep GAN framework (based on TensorFlow v2), the whole training process is parallelized to employ multi-node, multi-GPUs resources. The computations are performed on the Jülich DEEP-EST cluster by using four nodes, each hosting one NVIDIA Tesla V100 32GB GPU. This allows reducing the total wall training time from roughly 5 days to 28 hours.

A mini-batch size per GPU of 8 boxes, an initial learning rate of 10^{-4} and the ADAM optimizer are chosen based on previous optimizations [20].

4. Results

To inspect the achieved quality of the training, the GAN model, trained on the R2K1 configuration using both velocity and temperature fields, is initially tested on a in-sample snapshot, i.e., on data that are statistically equivalent to the training data. Figure 2 (a) shows the a-priori joint Probability Density Function (jPDF) of the GAN as SFS stress tensor closure model (Eq. (2)) that can be compared with the performance of the dynamic Smagorinsky model (Fig. 2 (b)). The data-driven model performs extremely well on data that are statistically equivalent to the training data, as there is a remarkable alignment with the diagonal, where the dynamic Smagorinsky model [25] exhibits a relatively low correlation. In this respect, the dynamic Smagorinsky model [25] is chosen as a reference due to its popularity and wide application [26], though it might be not optimal for such analysis. Possible suitable comparisons, for example, deconvolution methods based on the Taylor-series could be found in Hassanaly *et al.* [14]. Figure 2 (c) shows the a-priori performance of the GAN as SFS scalar flux closure model. The narrow spread over a wide range along the diagonal and the alignment of the bin cloud with the diagonal indicate that the GAN performs well. However, the model is not so accurate in predicting negative SFS scalar values, as the bins increasingly deviate from the diagonal. The results indicate that the training approach is successfully and the model can be used as reference model for the following investigations.

4.1. Generalization at different Reynolds numbers

To assess the generalizability of the trained GAN to different Reynolds numbers, the model obtained by training on the R2K1 configuration is used for the prediction of flames at different Reynolds numbers [21].

Fig. 3 shows the contour plots of the velocity magnitude of the F-DNS, the super-resolved field using the GAN network, and the DNS field of the R1K1 simulation, i.e., at decreased Re relative to the training dataset, providing just an intuitive metric to judge the reconstruction quality. The Root Mean Squared Error (RMSE) of the super-resolved fields is roughly 75% less than the RMSE of the F-DNS, demonstrating a considerable improvement. However, perceptually the SR field has still some textures that differ from the true DNS. This is reasonable as the whole training strategy has been developed to obtain sufficient physical accuracy, which may come at a trade-off with the perceptual quality. Hence, the model is able to reconstruct small-scale structures close to those from DNS fairly well. Figure 4 (a) shows the jPDF plot of one component of the SFS stress tensor computed using the GAN model trained on the R2K1 configuration and applied to the R1K1 dataset. There are no substantial differences when the model is applied to a lower *Re* configuration as the alignment with the diagonal is similar to the reference case. Moreover, Fig. 5 (a) shows the jPDF plot of one component of the SFS scalar flux. The decreased accuracy in predicting negative SFS scalar values is comparable to the R2K1 result, meaning that such behavior does not impact the generalization capability. Moreover, Fig. 4 (b) and Fig. 5 (b) show the same statistical quantities as for the previous investigation when the model is trained on R2K1 and applied to R4K1 configuration, i.e., to higher Re. Analogous conclusions can be drawn from this analysis, where Fig. 4 (b) shows a slightly worse correlation compared to the previous case. However, the overall trend does not reveal any major qualitative differences when the model is applied at different Reynolds numbers. Additional statistical quantities that support such analyses are included in the supplementary material. The analysis suggests that the network is able to reconstruct the velocity and temperature field of premixed jet flame configurations, extrapolating well at both lower and higher Re.

Among the four configurations, two different ratios are essentially conserved: the $\Delta/\eta \approx 8$ and $\Delta/\delta_L \approx 1.45$. Those might then represent ratios fundamental to achieve extrapolation capabilities, as it was previously found when predicting the progress variable variance [19]. The relative importance of these two parameters on the predictive capability is then analyzed on the following sections.

4.2. Generalization at higher Karlovitz number

A further generalization test in terms of Ka is performed. The previously trained model is used to predict the flow field of the R2K2 simulation, that has a Ka approximately 10 times larger than the data the model was trained on. Between the two datasets, only one of the previous ratios is strictly conserved, namely the $\Delta/\eta \approx 8$. Indeed, $\Delta/\delta_L \approx 0.062$ ratio is quite smaller compared to the training condition.To provide the reader with a sense of the relative performance of the model, the same statistics as shown before are reported. The performance of the GAN model as an a-priori SFS stress tensor closure model (Fig. 4(c)) is confirmed by the narrow spread over a wide range along the diagonal, and the alignment of the data with the diagonal. However, the data with lower probability are the ones with a larger distance from the diagonal compared to the other two analyses, i.e., Fig. 4(a) and Fig. 4(b). Moreover, the model has a similar tendency in predicting negative SFS values, where there are no quantitative differences compared to the reference case.

Despite the different thermo-physical properties between training and testing conditions, this result indicates that both velocity and temperature fields are reconstructed fairly consistently with the DNS data. Correct representation of turbulence dynamics, which

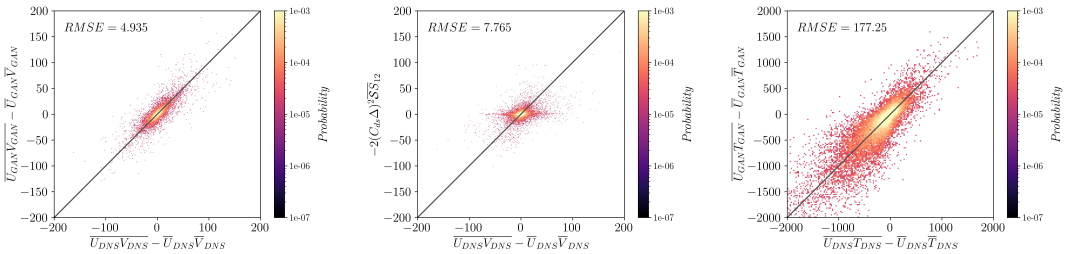

(a) (b) (c)

Fig. 2: jPDF plot of the subfilter-scale stress tensor component τ_{12}^r computed using the GAN model compared with the DNS result (a), jPDF plot of the subfilter-scale stress tensor component τ_{12}^r computed using the dynamic Smagorinsky model [2] compared with the DNS result (b), and jPDF plot of the subfilter-scale scalar flux component τ_1^T computed using the GAN model compared with the DNS result (c) for an in-sample snapshot of the R2K1 dataset.

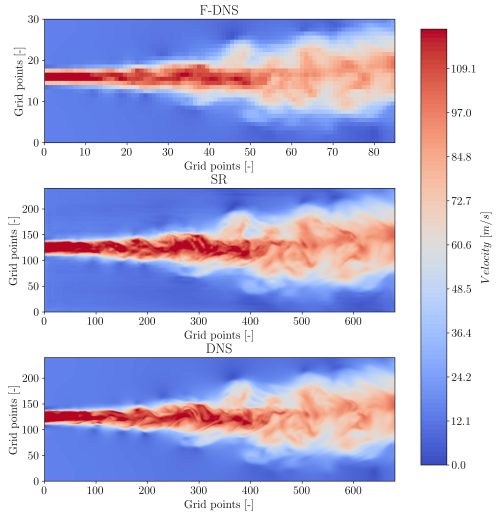

Fig. 3: Contour plot (sliced in the spanwise direction) of the velocity magnitude for the Filtered DNS field (F-DNS), super-resolved field using the GAN network (SR), and ground-truth (DNS) field of the R1K1 simulation.

strongly influences the transport of the scalar, indicates that the ratio Δ/δ_L might be not fundamental for generalizability.

To investigate further, the model trained on the R2K1 dataset is tested on the H2K2 jet flame, which presents the most general test performed. Although both datasets have comparable Ka and Re numbers, the ratios dx/η and dx/δ_L ratios are substantially different from those of the training dataset. Two independent approaches are performed. First, the testing dataset is filtered with a filter width of 8 in each direction, consistent with the training filter width. In this scenario, the ratios $\Delta/\eta \approx 14.88$ and $\Delta/\delta_L \approx 0.31$ are considered, which are substantially different from the training dataset. Figure 6 (above) shows the contour plots of the velocity magnitude. The GAN model strongly overpredicts the velocity in the jet region which results thicker and without small-scales turbulent oscillations, while the error is less marked in the coflow. This behavior is quantitatively confirmed by the Probability Density Function (PDF) of the normalized velocity gradient in Fig. 7 (above), where the GAN model tends to overpredict the large gradients.

As a counter test, the filter width is chosen to be consistent with the ratio $\Delta/\eta \approx 8$ used during the training, so that the filter size of 4 in each direction is employed leading to a ratio $\Delta/\eta \approx 6.6$ which is closer to that used during the training. Figure 6 (below) shows the same contour plots as before. The velocity magnitude of the SR field is increased or decreased resulting in a field that looks visibly sharper, where some features at the jet regions are enhanced. However, the model seems to under-resolve thin or fine features, which are bulkier and less detailed relative to the DNS field. This is partially due to the fact that the model can perform only an upsampling 8 (the one on which has been trained), so it is rather difficult to match the ratio Δ/η precisely.

The conclusions drawn from the previous analysis are bolstered by looking at the PDF of the normalized velocity gradient in Fig. 7 (below). The SR line marginally deviates from the DNS solution with a tendency to slightly underestimate the larger structures. This indicates that the ratio Δ/η needs to be conserved between training and application of the network. However, the Δ/δ_L ratio does not seems to be fundamental.

4.3. Generalization towards different physical quantities

To further explore the predictive capabilities of the GAN, the model previously trained on the R2K1 configuration using the three velocity components and temperature as input variables is employed to predict the OH mass fraction field of a snapshot of the same dataset, which was never seen during the training. As such quantity was not included during the training, the error of the SR field should be consistent throughout the entire field. This is however not the case. Fig. 8 depicts the contour plots of OH mass fraction on a sub-domain located at the center and $15H$ far from the inlet.

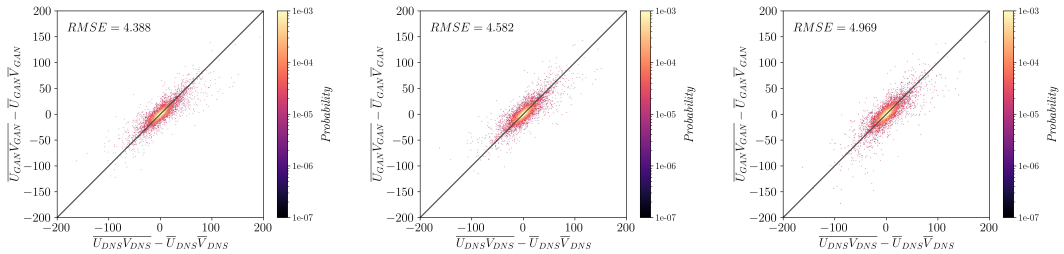

(a) (b) (c)

Fig. 4: jPDF plot of the subfilter-scale stress tensor component τ_{12}^r computed using the GAN model when trained on the R2K1 configuration and evaluated on R1K1 (a), R4K1 (b), and R2K2 (c) datasets.

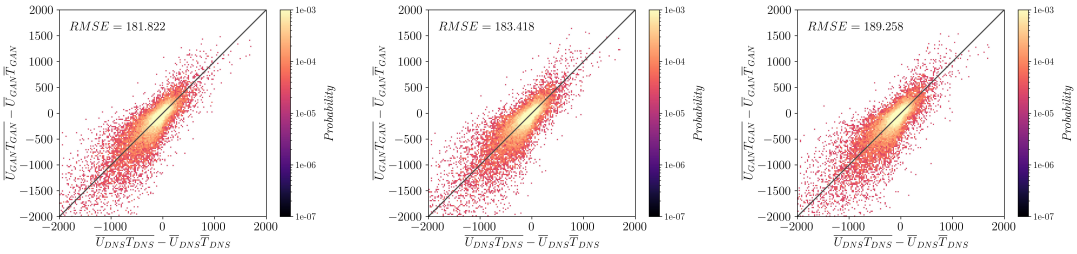

(a) (b) (c)

Fig. 5: jPDF plot of the subfilter-scale scalar flux streamwise component τ_1^T computed using the GAN model when trained on the R2K1 configuration and evaluated on R1K1 (a), R4K1 (b), and R2K2 (c) datasets.

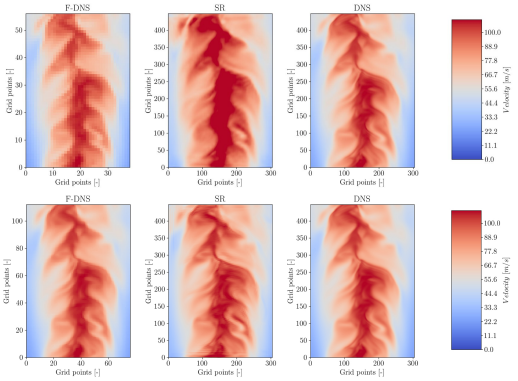

Fig. 6: Contour plot (sliced in the spanwise direction) of the velocity magnitude for the Filtered DNS field (F-DNS), super-resolved field using the GAN network (SR), and ground-truth (DNS) field of the H2K2 simulation keeping the filter size consistent with the training strategy (above) and keeping the Δ/η ratio consistent with the training strategy (below).

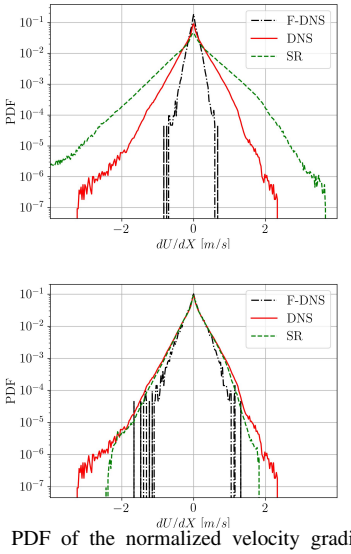

Fig. 7: PDF of the normalized velocity gradient in the streamwise direction on the H2K2 simulation keeping the filter size consistent with the training strategy (above) and keeping the Δ/η ratio consistent with the training strategy (below).

The coflow and the central jet regions with nearly constant values, are captured rather poorly and the error is exacerbated relative to the F-DNS as non-physical oscillations are introduced. However, at the boundary between the jet and the coflow, where the majority of heat is released and the gradients of the scalar fields are the most profound, the error is clearly mitigated, and the network creates structures that are almost alike the DNS. Such behavior could be explained by the link between the OH mass fraction and the velocity fields as indicated by Barwey *et al.*[27]. The results obtained might be a consequence of the gradient loss term $\mathrm{L}_{\mathrm{gradient}}$ and may highlight the need to move beyond simple pixel-loss approaches if physically accurate fields are desired. The capability of GAN to predict quantities having different values and dynamics than those used for the training is promising, although this would need a deeper study in future work.

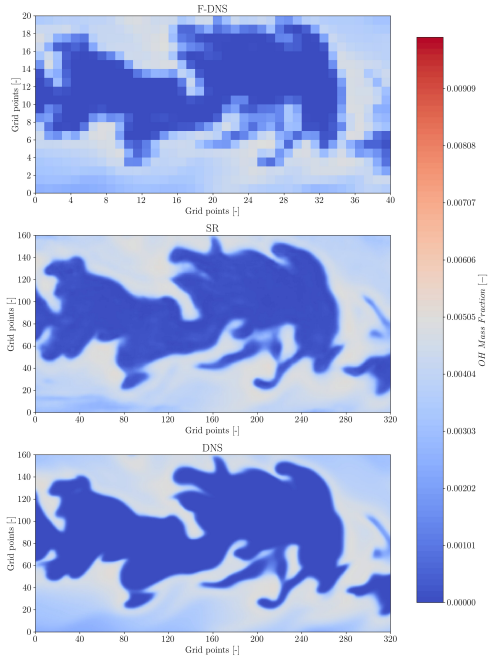

Fig. 8: Contour plot of the OH mass fraction for the Filtered DNS field (F-DNS), super-resolved field using the GAN network (SR), and ground-truth (DNS) field of the sub-domain of the R2K1 simulation (sliced in the spanwise direction)

4.4. Discussion of the results obtained

The results obtained indicate that the GAN can be employed as an accurate a-priori subfilter-scale model only when the ratio Δ/η is consistently ensured between training and testing conditions. The prediction capabilities deteriorate when such a key parameter is not conserved; early tests had shown that there was a consistent over- or under-prediction of the reconstructed fields in such a case. This represents a challenge for ML models that requires further understating, as recently reported by Attili *et al.* [18]. In addition, as the LES-to-DNS grid ratio and the filter width are fixed in the network architecture and set before even training the GAN, additional investigations are required to achieve superior generalization capabilities. This restriction to relying on a single value of Δ/η may be relaxed by training the GAN model on a range of filter size values. Moreover, while the a-priori generalization capabilities obtained are promising, memory limitations must be taken into account in the upsampling of three-dimensional fields. Furthermore, the analyses conducted must be confirmed through a-posteriori LES investigations in which the GAN model is embedded into numerical solvers.

5. Conclusions

A super-resolution GAN has been employed to model the unresolved subfilter-scale stresses and scalar flux for LES of premixed combustion. A turbulent methane/air premixed jet flame has been considered for the training, using as input the three velocity components and the temperature field. A-priori analyses have shown that the model performs extremely well when applied to in-sample data, indicating that the training approach was successfully executed and the trained model could be used as reference. The capability of the GAN model to extrapolate at either lower and higher Re has been demonstrated using a set of four methane/air premixed flames. As the ratio between the filter width and the Kolmogorov scales, Δ/η, was unchanged, the GAN model predicted accurately the subfilter-scale stress tensor and scalar flux. Promising extrapolation towards a higher Karlovitz number was further demonstrated on similar and rather disparate flame conditions indicating the importance of preserving the ratio Δ/η. Though, the ratio between the filter size and thermal flame thickness, Δ/δ_L, appeared to be a less relevant parameter to be conserved. In addition, the GAN model showed promising results also in the prediction of scalar quantities, e.g., a species mass fraction, different from those used during the training, showing that the model was able to reconstruct scalar fields with large gradients.

Additional a-priori investigations of such extrapolation capabilities, fundamental for universal closure models, are recommended since the performance of DL models to far-from-training conditions is still mainly unexplored. For instance, the presented results do not consider the performance below the critical Karlovitz number where the impact of the flame thickness might be fundamental. Similarly, generalization to different fuels is advised. Finally, the work highlights the importance of interpreting DL models suggesting the development of physical-inspired architectures and the need to confirm those conclusions through a-posteriori LES simulations, in which the interaction of the model with the intrinsic numerical errors in CFD solvers could provide further challenges.

Acknowledgments

The research leading to these results has received funding from the EU's Horizon 2020 research and innovation program under the Center of Excellence in Combustion project (CoEC), grant agreement no. *952181*, and from the German Federal Ministry of Education and Research (BMBF) and the state of North Rhine-Westphalia for supporting this work as part of the NHR funding. The authors gratefully acknowledge the computing resources from the DEEP-EST project, which received funding from the EU's Horizon 2020 research and innovation program under the grant agreement no. *754304*. We thank Mr. Sedona for the support in the porting of the application.

References

[1] H. Pitsch, Large-eddy simulation of turbulent combustion, Annu. Rev. Fluid Mech. 38 (2006) 453–482.

[2] T. Poinsot, D. Veynante, Theoretical and numerical combustion, RT Edwards, Inc., 2005.

[3] L. Zhou, Y. Song, W. Ji, H. Wei, Machine learning for combustion, Energy and AI (2021) 100128.

[4] M. Ihme, W. T. Chung, A. A. Mishra, Combustion machine learning: Principles, progress and prospects, Progress in Energy and Combustion Science 91 (2022) 101010.

[5] S. L. Brunton, B. R. Noack, P. Koumoutsakos, Machine learning for fluid mechanics, Annual Review of Fluid Mechanics 52 (2020) 477–508.

[6] A. Vollant, G. Balarac, C. Corre, Subgrid-scale scalar flux modelling based on optimal estimation theory and machine-learning procedures, Journal of Turbulence 18 (9) (2017) 854–878.

[7] A. Seltz, P. Domingo, L. Vervisch, Z. M. Nikolaou, Direct mapping from LES resolved scales to filtered-flame generated manifolds using convolutional neural networks, Combustion and Flame 210 (2019) 71–82.

[8] S. Yellapantula, B. A. Perry, R. W. Grout, Deep learning-based model for progress variable dissipation rate in turbulent premixed flames, Proceedings of the Combustion Institute 38 (2) (2021) 2929–2938.

[9] S. Yao, B. Wang, A. Kronenburg, O. Stein, Conditional scalar dissipation rate modeling for turbulent spray flames using artificial neural networks, Proceedings of the Combustion Institute 38 (2) (2021) 3371–3378.

[10] C. J. Lapeyre, A. Misdariis, N. Cazard, D. Veynante, T. Poinsot, Training convolutional neural networks to estimate turbulent sub-grid scale reaction rates, Combustion and Flame 203 (2019) 255–264.

[11] X. Wang, K. Yu, S. Wu, J. Gu, Y. Liu, C. Dong, Y. Qiao, C. Change Loy, Esrgan: Enhanced super-resolution generative adversarial networks, in: Proceedings of the European conference on computer vision (ECCV) workshops, 2018, pp. 0–0.

[12] C. Ledig, L. Theis, F. Huszár, J. Caballero, A. Cunningham, A. Acosta, A. Aitken, A. Tejani, J. Totz, Z. Wang, W. Shi, Photo-realistic single image super-resolution using a generative adversarial network, in: 2017 IEEE Conference on Computer Vision and Pattern Recognition (CVPR), 2017, pp. 105–114. doi:10.1109/CVPR.2017.19.

[13] K. Fukami, K. Fukagata, K. Taira, Super-resolution reconstruction of turbulent flows with machine learning, Journal of Fluid Mechanics 870 (2019) 106–120.

[14] M. Hassanaly, A. Glaws, K. Stengel, R. N. King, Adversarial sampling of unknown and high-dimensional conditional distributions, Journal of Computational Physics 450 (2022) 110853.

[15] M. Bode, M. Gauding, Z. Lian, D. Denker, M. Davidovic, K. Kleinheinz, J. Jitsev, H. Pitsch, Using physics-informed enhanced super-resolution generative adversarial networks for subfilter modeling in turbulent reactive flows, Proceedings of the Combustion Institute 38 (2) (2021) 2617–2625.

[16] T. Grenga, L. Nista, C. Schumann, A. N. Karimi, G. Scialabba, A. Attili, H. Pitsch, Predictive data-driven model based on generative adversarial network for premixed turbulence-combustion regimes, Combustion Science and Technology 0 (0) (2022) 1–24.

[17] C. Lapeyre, A. Misdariis, N. Cazard, T. Poinsot, A-posteriori evaluation of a deep convolutional neural network approach to subgrid-scale flame surface estimation, in: Proceedings of the Summer Program 2018. Center for Turbulence Research, 2018, pp. 349–358.

[18] A. Attili, N. Sorace, L. Nista, C. Schumann, A. N. Karimi, G. Scialabba, T. Grenga, H. Pitsch, Investigation of the extrapolation performance of machine learning models for LES of turbulent premixed combustion, in: 10th European combustion meeting, 2021, pp. 460–465.

[19] V. Xing, C. Lapeyre, T. Jaravel, T. Poinsot, Generalization capability of convolutional neural networks for progress variable variance and reaction rate subgrid-scale modeling, Energies 14 (16) (2021) 5096.

[20] L. Nista, C. K. D. Schumann, G. Scialabba, T. Grenga, A. Attili, H. Pitsch, The influence of adversarial training on turbulence closure modeling, in: AIAA SCITECH 2022 Forum, 2022, pp. 1–9.

[21] A. Attili, S. Luca, D. Denker, F. Bisetti, H. Pitsch, Turbulent flame speed and reaction layer thickening in premixed jet flames at constant karlovitz and increasing reynolds numbers, Proceedings of the Combustion Institute 38 (2) (2021) 2939–2947.

[22] T. Grenga, J. F. MacArt, M. E. Mueller, Dynamic mode decomposition of a direct numerical simulation of a turbulent premixed planar jet flame: convergence of the modes, Combustion Theory and Modelling 22 (4) (2018) 795–811.

[23] A. Attili, K. Kleinheinz, D. Denker, L. Berger, F. Bisetti, H. Pitsch, Mixing and entrainment of burned products in high karlovitz number premixed jet flames, in: Proceeding of the European Combustion Meeting, Lisbon, Portugal, 2019, pp. 1–5.

[24] J. F. MacArt, T. Grenga, M. E. Mueller, Effects of combustion heat release on velocity and scalar statistics in turbulent premixed jet flames at low and high karlovitz numbers, Combustion and Flame 191 (2018) 468–485.

[25] J. Smagorinsky, General circulation experiments with the primitive equations: I. the basic experiment, Monthly weather review 91 (3) (1963) 99–164.

[26] Z. Nikolaou, C. Chrysostomou, Y. Minamoto, L. Vervisch, Evaluation of a neural network-based closure for the unresolved stresses in turbulent premixed v-flames, Flow, Turbulence and Combustion 106 (02 2021).

[27] S. Barwey, M. Hassanaly, V. Raman, A. Steinberg, Using machine learning to construct velocity fields from oh-plif images, Combustion Science and Technology (2019) 1–24.